ELSEVIER

Sensors and Actuators B 45 (1997) 19–26

SENSORS AND ACTUATORS B CHEMICAL

Thermal modelling and characterisation of micropower chemoresistive silicon sensors

Andrew Pike, Julian W. Gardner *

Department of Engineering, University of Warwick, Coventry, CV4 7AL, UK

Received 23 April 1997; received in revised form 28 July 1997; accepted 29 July 1997

Abstract

There is considerable interest in the development of low-cost, low-power resistive sensors for possible application in hand-held gas monitors. In this paper we describe the fabrication of a high-temperature, resistive sensor using silicon microtechnology which lies on a sub-micron thick membrane with an embedded platinum resistance heater. A thermal model of this micro-hotplate is constructed and compared with its observed behaviour. The microsensor can be operated at temperatures of up to 600°C and has a low d.c. power consumption per sensor of 40 mW at 300°C. As the thermal time-constant of the microsensor is only about 5 ms, its average power consumption can be reduced by a factor of at least ten through an a.c. mode of operation, thus making a single device or even an array device suitable for battery-powered instruments. © 1997 Elsevier Science S.A.

Keywords: Thermal sensor; Gas sensor; Micro-hotplates; Micro-filament

1. Introduction

An increasing degree of integration is being designed into sensor systems in order to meet a growing demand for portable instrumentation. Low power consumption is a fundamental requirement for a sensor with an acceptable battery life-time, e.g. 12 h. An application of key interest here is the development of a portable gas (or vapour) monitor for use in manufacturing, automotive, environmental monitoring and medical industries. The growth of this market has been limited both by the relatively high power consumption of current commercial chemical sensors (e.g. pellistors require 350–850 mW [1] and Taguchi gas sensors require 230–760 mW [2]) and by the high cost of the manufacturing technology. However, the application of silicon microtechnology, which has revolutionised the microelectronics industry over the last 20 years, may permit the desired benefits, i.e. miniaturisation, low power, reproducibility and low unit-cost [3]. Moreover, the lower power consumption from such an advance in technology would permit the use of an array of gas sensors which would then provide the additional benefits of improved selectivity and greater stability.

A common type of chemical sensor exploits a change in the electrical resistance of a material on exposure to a gas, which is often referred to as *chemoresistive*. The resistance of a chemoresistor is measured electrically usually by passing a d.c. current through a gas-sensitive material and measuring the voltage developed across two contact electrodes. For many gas-sensitive materials, the sensor's performance is enhanced at higher temperatures, e.g. tin oxide films are typically operated in the range of 300–600°C. The use of silicon microtechnology enables both the gas sensor and electrical heating element to be integrated onto the same chip. Furthermore, silicon technology has been advanced by the recent development of bulk and surface micromachining techniques, which not only allow three-dimensional structures to be fabricated but also provide benefits of better reproducibility in batch processing. Micromachining techniques are now being used in the manufacture of a variety of sensors in order to improve their performance. For example, a low power CO sensor has been reported by Grisel [4] which is a planar chemoresistive device based on a thin film of tin oxide on a heated substrate. Such a structure will be referred to here as a 'micro-hotplate'.

* Corresponding author. Tel.: +44 1203 523523; fax: +44 1203 418922; e-mail: j.w.gardner@warwick.ac.uk

PII S0925-4005(97)00261-X

In this paper we report on the design and thermal characterisation of a novel, low-power silicon chemoresistor employing a micro-hotplate structure. An electrical lumped-element model of the structure has been constructed to aid in its characterisation.

2. Fabrication details

The general structure of the integrated chemoresistor and micro-hotplate is shown in Fig. 1. A set of five mask-plates was required to process the silicon wafers and hence fabricate the devices [5]. The micro-hotplate comprises a 200 nm film platinum (Pt) resistance micro-heater embedded between two 250 nm layers of low-stress silicon-rich silicon nitride (SiN_x). 80 nm of thermal oxide was deposited before the low pressure chemical vapour deposition (LPCVD) of SiN_x in order to help minimise any residual stress in the membrane. A KOH anisotropic back-etch was then used to form the micromachined membrane (3.24 by 1.11 mm) with a centrally located heated area (1.35 by 0.37 mm). The chemoresistive elements were formed on the micro-hotplate surface, by depositing a gas-sensitive material over 300 nm thick gold (Au) electrodes patterned by a lift-off process. 10 nm layers of tantalum and titanium were used to seed the Pt and Au layers, respectively. Finally, a special hard-baked photoresist was used to protect the interconnnects and act as a chemically-protective layer.

The electrical, mechanical and thermal design of the device makes it suitable for the deposition and operation of a number of different gas-sensitive materials [5], such as drop-coated thick films of pure, Pt-doped and Pd-doped SnO_2 held at 300–500°C [6], metal-substituted phthalocyanine films held at 100–300°C, and electroplated conducting polymers films held close to ambient, i.e. < 100°C [7]. Since these gas-sensitive materials can be deposited *after* the wafers have been processed, and annealed (where necessary) on the chip, it is possible to produce a hybrid array sensor (e.g. a device with more than one sensor employing different sensing materials) with very little effort.

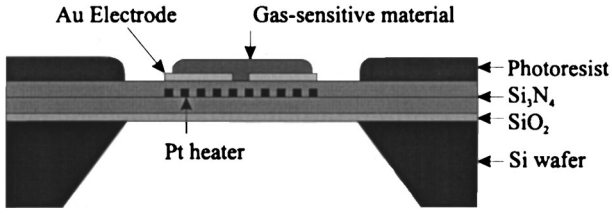

Fig. 1. Cross-section of the basic design of the high-temperature gas microsensor: a platinum resistive heater is embedded within silicon nitride layers to form a 'micro-hotplate' while gold electrodes sense the electrical resistance of the gas-sensitive material. (The ultra-thin metallisation seeding layers are not shown for the sake of clarity).

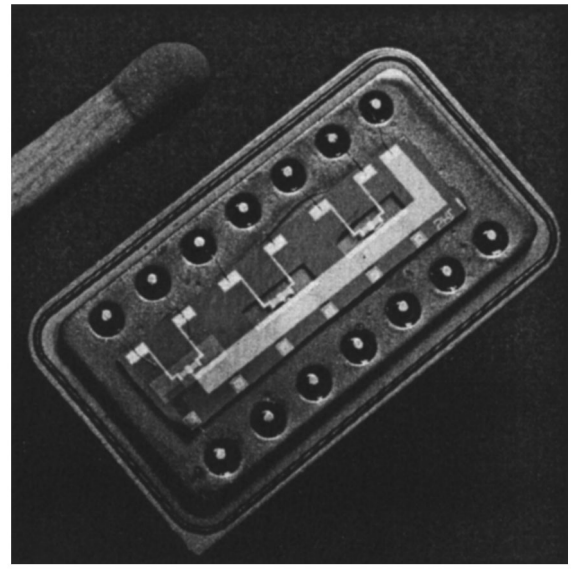

Fig. 2. Photograph of the linear array gas microsensor (referred to by SRL125/MOS) mounted on a 0.1″ pitch 14-pin d.i.l. metal header and comprising three micro-hotplates (translucent regions) with embedded platinum micro-heaters. Each micro-hotplate supports a pair of interdigitated sensing electrodes with a common ground line (thick track).

The basic device described here consists of three micro-hotplates with a linear array of six chemoresistors, arranged in pairs on each membrane, as shown in Fig. 2. The aspect ratio of the gold sensing electrodes was varied according to the electrical conductivity of the gas-sensitive film.

3. Thermal characteristics

A block diagram illustrating the signal conversion by the micro-hotplate is shown in Fig. 3. In our model we have made two assumptions; first, the thermal response time of the micro-hotplate is much slower than that of the Pt micro-heater so that the thermal time constant of the micro-heater can be neglected; and secondly, the heat lost within the structure is assumed to be negligible and therefore, since it is an ultra-thin membrane, the gas-sensitive material above the heater will be at a uniform temperature (T) which will be the same as the micro-heater temperature (T_H) in the steady-state.

In order to control the temperature of the micro-hotplate surface, it is necessary to characterise the relationship between the resistance of the micro-heater and its

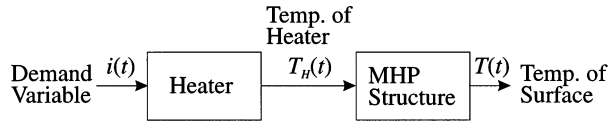

Fig. 3. Block diagram of signal conversion by the micro-hotplate.

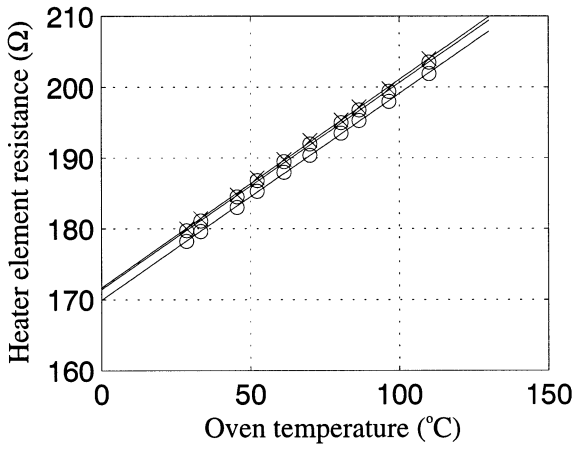

Fig. 4. Diagram showing the linear temperature-dependence of three platinum micro-heaters within the gas microsensor.

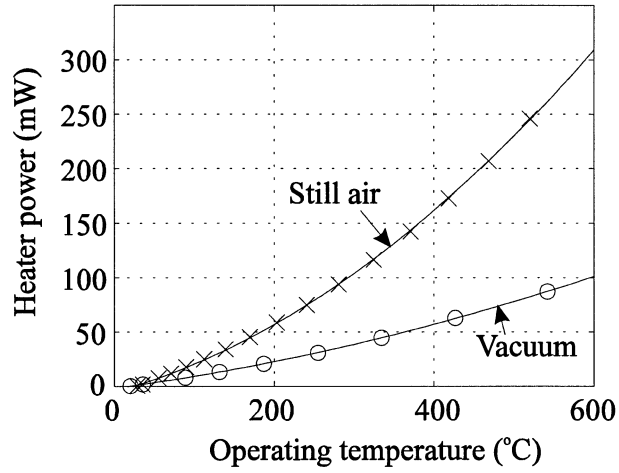

Fig. 5. Power consumption of the micro-hotplate in still air and in a vacuum (10^{-5} Torr) at different operating temperatures. The experimental data-points have been fitted to second-order polynomials with $T_a = 29$°C.

operating temperature. All three micro-heaters in the linear array device were calibrated over a temperature range of ambient temperature to about 150°C in a temperature-controlled (± 1°C) oven. The micro-heater resistances were measured by a Maplin M-4510 digital multimeter (DMM). Typical resistance-temperature plots of the three microheaters are shown in Fig. 4. These results are well described by a first-order function which corresponds to the well-known temperature dependent expression for the resistance of metals, i.e.

$$R_H(T) = R_0[1 + \alpha(T - T_a)] \quad (1)$$

where R_H is the resistance of the micro-heater at temperature T, R_0 its resistance at ambient temperature T_a, and α is the linear temperature coefficient of resistance. The values of α for each micro-heater were calculated from the gradient of the plots ($R_0\alpha$) shown in Fig. 4, and were found to be $(2.03 \pm 0.05) \times 10^{-3}$°C^{-1}.

3.1. Steady-state power loss

Electrical power supplied to the micro-heater can be dissipated by three heat loss mechanisms: conduction to the surrounding structure; conduction to air; and by radiation. The conductive heat losses to air are dissipated by convection and as such, for the sake of expedience, are referred to here as convective losses. When the micro-hotplate reaches its steady-state operating temperature, the electrical power consumption must be equal to the total thermal loss. This steady-state power consumption was measured by driving a constant current (with a Knick Current Calibrator, Model J152) through the heater element and recording the voltage developed across it (with a DMM). The current (I) and voltage (V) characteristics allow the electrical power ($I \times V$) and the heater resistance (V/I) to be calculated. Whereupon, the resistance can be used to calculate the operating temperature via Eq. (1). The calibration line of the heater was assumed to have only a small extrapolation error ($\sim \pm 1\%$ up to 770°C) because platinum is known to be extremely linear over the temperature range of interest (ambient to 600°C). Plotting the heater power against operating temperature allows the thermal performance of the micro-hotplate to be determined. The magnitude of contributions to the total thermal power loss by conduction and radiation have also been investigated by measuring the power consumption under a vacuum pressure of 10^{-5} Torr after mounting the micro-hotplate in a thin film evaporator unit (Bir-Vac). This method removes the convective heat loss component. The results allow a comparison of the thermal power losses in still air and in a vacuum as shown in Fig. 5. It is evident from the figure that the power consumption of the micro-hotplate in still air is very low (e.g. 160 mW at 400°C)—particularly as this represents a pair of resistive sensors. The magnitude of convective heat loss in air can be determined from the difference between these two measurements. Whereas, the theoretical radiation power loss, which is expected to be small over the temperature range of interest here, has been calculated using the Stefan–Boltzmann law [8],

$$P_r(T) = \epsilon\sigma A(T_H^4 - T_a^4) \quad (2)$$

where P_r is the net power radiated out of a body, A is the heated area, ϵ is the effective emissivity of the surface, and σ is the Stefan–Boltzmann constant (56.7×10^{-9} W m^{-2} K^{-4}). Assuming the micro-hotplate surface is a black body radiator[1] (i.e. $\epsilon = 1$) and emits radiation from a heater area A_h of 5.0×10^{-7} m^2

[1] Normal total emittance of silicon nitride is typically around 0.9 between 300 and 900 K.

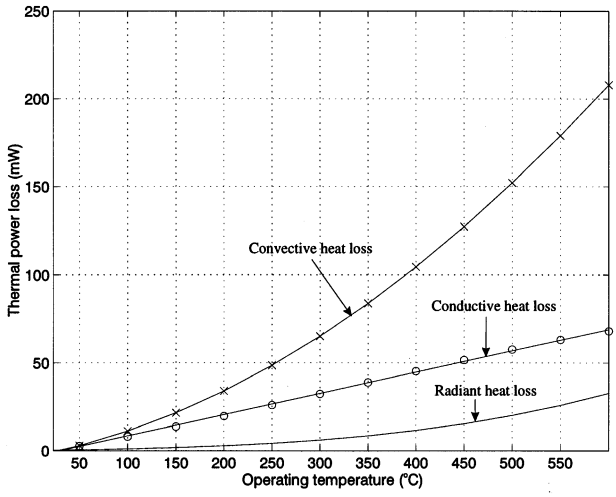

Fig. 6. Estimates of the conductive and convective heat losses of the micro-hotplate (SRL125/MOS) from the power losses measured in air and vacuum (see Fig. 5). The theoretical radiation loss has been calculated and is also shown for comparison.

(this area has to be doubled to obtain A because radiation is emitted from both sides of the micro-hotplate), the theoretical value of P_r can be subtracted from the heater power measured in a vacuum to obtain an estimate of the conductive power loss (P_m). The various thermal power losses due to convection (P_a), conduction and radiation losses are shown in Fig. 6.

From Fig. 6, it is evident that the experimentally-derived conductive power loss is well described by a first-order expression, where

$$P_m(T_H) \approx [P_H(\text{vacuum}) - P_r] = 0.123(T_H - T_a) \quad (3)$$

with the ambient temperature, T_a, having a value of 28.9°C. Similarly, the experimentally-derived convective power loss can be described by a second-order polynomial, namely

$$P_a(T_H) \approx [P_H(\text{air}) - P_H(\text{vacuum})] = 0.104(T_H - T_a) + 4.129 \times 10^{-4}(T_H^2 - T_a^2) \quad (4)$$

where T_a takes the same value as before.

It is also clear from the experimental data that the convective heat loss is a significant proportion (about 2/3) of the total heat loss P_H of the micro-hotplate above a temperature of 50°C or so. The convective heat loss may thus be significantly affected by choosing to mount the device upside down with the gas passing slowly below the micro-hotplate—usually outside a protective, flame-resistant, metal mesh in commercial gas sensors. This physical arrangement should make it more difficult for the thermal air currents to move and thus reduce the amount heat transferred from the active surface to the air.

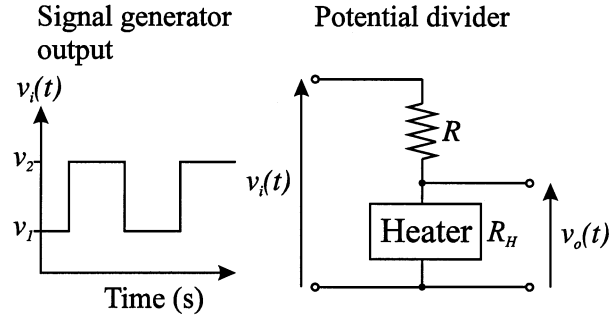

Fig. 7. A potential divider circuit (right) was used to measure the characteristic response $v_0(t)$ of the platinum micro-heater to a square-wave driving voltage (left), $v_i(t)$.

3.2. Transient characteristics

The transient response of the micro-hotplate was determined by placing the micro-heater resistor (R_H) in series with a precision metal film reference resistor (R) of 100.26 Ω to form a potential divider circuit. A square wave with a variable d.c. offset was applied to the potential divider by a function generator (Thandor, TG501, supplied by R.S.), as shown in Fig. 7. The transient response, i.e. device voltage $v_0(t)$, was measured in the time domain using a Control Systems Analyser (Hewlett Packard, 3563A), as shown in Fig. 8. From the observed transient behaviour of the micro-heater (see Fig. 8), the system can be described by a first-order model that neglects the switching spikes. The energy storing element in the system can then be assumed to be associated with the thermal nature of the micro-hotplate. Hence, the transient signals can be analysed to obtain the thermal time constant of the micro-hotplate, i.e. the time taken for a transient signal to reach 63% of the final steady-state value. With respect to Fig. 8, the minimum and maximum voltages are 3.355 and 3.940 V, which correspond to operating temperatures of 228.7 and 275.8°C, respectively. The

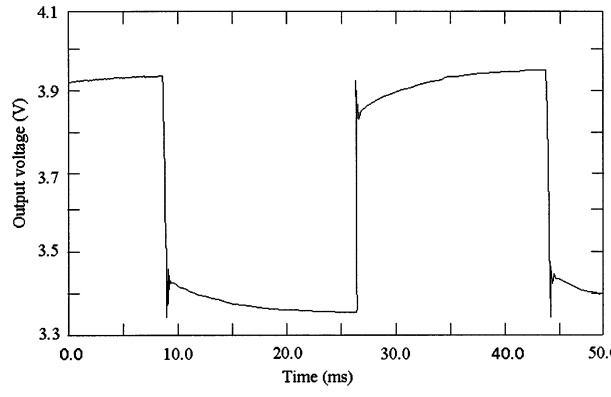

Fig. 8. Observed transient response of the micro-heater to a square wave drive voltage with a frequency of about 30 Hz. The average operating temperature of the micro-hotplate was 252°C.

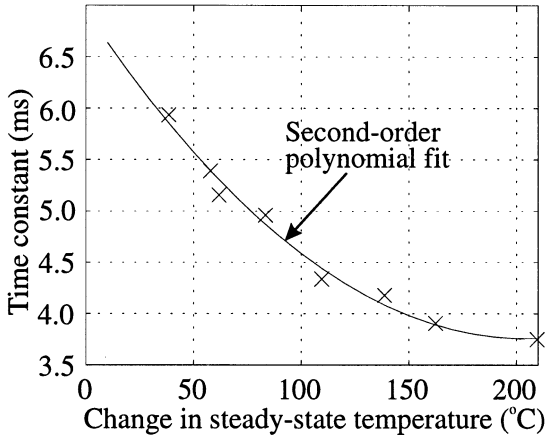

Fig. 9. Effect of the magnitude of the temperature excursion on the thermal time constant of the micro-hotplate.

time constant τ associated with reaching the limiting values was measured to be 4.336 ms.

The relationship between the time constant and operating temperature of the micro-hotplate was investigated further by applying a higher square-wave peak-to-peak voltage and hence generating larger temperature swings. The characteristic curve is shown in Fig. 9 in which the thermal time constant falls with increasing temperature. This is probably because the ratio of the thermal conductivity to heat capacity of the silicon nitride membrane increases with increasing temperature and thus enhances the dynamics.

4. Lumped-element model of a micro-hotplate

Numerical modelling of the micro-hotplate was undertaken both to understand the thermal characteristics reported in the previous section and to help in the design of new micro-structures. To this end, the microstructure was sub-divided into a set of lumped volumes with a constant temperature and each represented by a node; the heat balance equations can be described between adjacent nodes.

The total heat flow (q) between two adjacent nodes can be written as,

$$q = \frac{(T_1 - T_2)}{R_{\text{th}}} \tag{5}$$

where $(T_1 - T_2)$ is the temperature difference between the two nodes and R_{th} is the thermal resistance. Thermal conduction between adjacent volumes can be described by a thermal resistance, i.e.

$$R_{\text{cond}} = \frac{\delta x}{\kappa A_{\text{k}}} \tag{6}$$

where δx is the distance between the two nodes, κ is the thermal conductivity and A_{k} is the cross-sectional area of contact between the two volumes (normal to the one-dimensional co-ordinate x).

This expression suggests that an electrical analogy can be constructed. The existence of convective losses from the structure surface exposed to an ambient gas may be accounted for by adding to the network another node representing the gas. The thermal connection between these two nodes can again be represented by a thermal resistance according to,

$$R_{\text{th}} = \frac{1}{hA_{\text{c}}} \tag{7}$$

where h is the heat-transfer coefficient and A_{c} represents the surface area exposed to the convecting gas.

For transient modelling, the heat storage of each lumped nodal element must be taken into account. Continuing with the electrical analogy, the heat storage is represented by an electrical capacitor connected between the node and the ambient temperature node. This electrical capacitance is recognised as the thermal capacity of the lumped volume surrounding the node, according to

$$C = V\rho c_{\text{p}} \tag{8}$$

where V is the volume of the lumped element, ρ is the material density and c_{p} is the specific heat property of the material. Therefore, a simplified lumped-element model of our micro-hotplate has been used to construct an analogous circuit, as shown in Fig. 10. The components shown in Fig. 10 (b) are: T_{H} and T_{a}, the temperatures of the micro-heater and ambient surroundings; C the thermal capacitance of the micro-heater region; G_{cr} a thermal conductance associated with convection and radiation losses from the heated area; and R_{1-4} the resistances through the membrane due to thermal conduction from the heater node to the four nodes on the edge of the silicon support. This equivalent circuit assumes that the silicon support to the membrane, and the gas surrounding the membrane are both at ambient

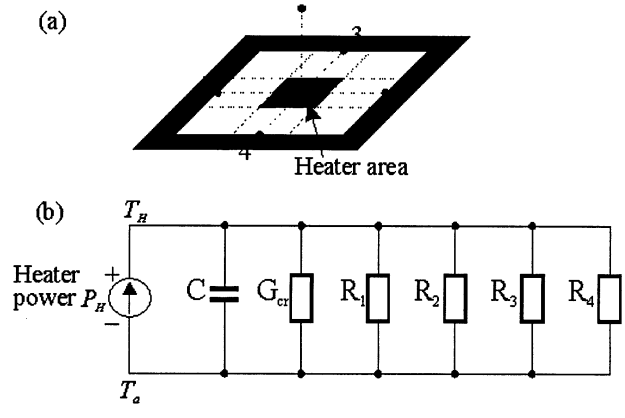

Fig. 10. (a) Diagram of the nodal subdivision of the heater area and silicon nitride membrane, and (b) its electrical analogue.

temperature (i.e. equivalent to electrical ground), and that convection and radiation losses are minimal outside of the heater area. These assumptions define the boundary conditions for the model. However, this lumped model does not take account of either heat conduction through the corner regions of the membrane or thermal convection outside the heated area. The components used in the thermal model are dependent on the geometry and the thermal properties of the lumped membrane.

The model can be expressed by the heat flow at the membrane node, according to,

$$C\frac{\mathrm{d}\,T_{\mathrm{H}}}{\mathrm{d}\,t} = P_{\mathrm{H}} - \Delta T\left(\frac{1}{R_1}+\frac{1}{R_2}+\frac{1}{R_3}+\frac{1}{R_4}+G_{\mathrm{cr}}\right) \tag{9}$$

where ΔT is defined as $(T_{\mathrm{H}} - T_{\mathrm{a}})$.

The total conductive thermal loss R_{cond} can be expressed as the parallel combination of the individual conductive resistances in terms of the membrane geometry, according to,

$$R_{\mathrm{cond}} = \frac{1}{\kappa m}\left(\frac{u_1 u_2}{4(u_1 a_1 + u_2 a_2)}\right) \tag{10}$$

where m is the membrane thickness, u_1 and u_2 are the long and short side lengths of the membrane, respectively. Similarly, a_1 and a_2 are the side lengths of the heated area.

The measured conductive losses described in Eq. (3) generates a value for $1/R_{\mathrm{cond}}$ of 123 mW K^{-1}. Substituting the measured value of $\mathrm{R}_{\mathrm{cond}}$ and the micro-hotplate dimensions into Eq. (10), gives $\kappa m = 22.74$ mW K^{-1}. This value can be compared to the theoretical κm derived from effective medium theory. The membranes are composed of 80 nm of SiO_2 and 500 nm of Si_3N_4 which have κ values of 1.4 and 28 W m^{-1} K (at 300 K), respectively. These values only account for 17 mW K^{-1} of the total κm measured. Hence, the effect of the gold electrodes on the membrane must be taken into account. An equivalent 66 nm Au layer compensates for the difference in κm.

The lumped model component, G_{cr}, can be expressed in terms of the convection (G_{c}) and radiation (G_{r}) losses, using Eqs. (2) and (7), according to,

$$G_{\mathrm{cr}} = G_{\mathrm{c}} + G_{\mathrm{r}} = 2A[h\Delta T + \epsilon\sigma(T_{\mathrm{H}}^4 - T_{\mathrm{a}}^4)] \tag{11}$$

where the heater area A is multiplied by a factor of two to account for the losses from both sides of the membrane. However, it is evident from the measured characteristics that the convection losses are second-order, as described by Eq. (4), hence h is not a constant. Therefore, to improve the accuracy of the model, the coefficient h is replaced by a first-order function of ΔT, according to,

$$h = 414.8\Delta T + 1.04 \times 10^5 \tag{12}$$

Similar compensation was required for the micro-hotplates's thermal capacitance, which is theoretically described by Eq. (8). The lumped value of C is theoretically the sum of the individual layer capacitances. However, since the c_{p} of SiO_2 and Si_3N_4 are approximately the same at 300 K, ~700 J kg^{-1} K, this value was used assuming a lumped Si_3N_4 membrane (580 nm thick) with $\rho = 3000$ kg m^{-3}. Substituting these values into Eq. (8) for the micro-hotplate geometry, generates a value of 6.06×10^{-7} J K^{-1} for C. The accuracy of this value can be assessed by considering the measured transient response, since the time constant of a first-order system is RC. The value of R is calculated by the application of the parallel combination of the thermal resistance components G_{cr} and G_{cond}. Using Eqs. (8) and (10)–(12), at an operating temperature of 276°C gives a theoretical time constant of 1.65 ms, compared to the measured value of 4.34 ms. The difference between the theoretical and observed values of τ can be described by adjusting the value of the thermal capacitance C in our model[2] from the expected value of 6.06×10^{-7} J K^{-1}. The theoretical value of R_{th} consistent with the experimental data is 2.87×10^3 (K W^{-1}), which produces a value of C 1.5×10^{-6} J K^{-1}—nearly twice the expected value of C. Dividing this value by the micro-heater area A_{h}, derives a capacitance per unit area of »3.0 J K^{-1} m^2. This can now be used as a model coefficient, replacing C by $3A_{\mathrm{h}}$. The lumped element model for the device design illustrated in Fig. 1 can now be represented in terms of micro-hotplate geometry and temperature, according to

$$\begin{aligned} 3a_1a_2\frac{\mathrm{d}\,T}{\mathrm{d}\,t} &= 2a_1a_2(412.9\Delta T^2 + 1.04\times 10^5\Delta T \\ &\quad + \sigma(T_{\mathrm{H}}^4 - T_{\mathrm{a}}^4)) \\ &= \left[\frac{9.1\times 10^2(u_1a_1 + u_2a_2)}{u_1u_2}\right] - P_{\mathrm{H}} \end{aligned} \tag{13}$$

where heater area is defined by $a_1 \times a_2$ and the larger nitride membrane by $u_1 \times u_2$.

The steady-state accuracy of this model was investigated by setting the left hand side of Eq. (13) to zero. The theoretical thermal power loss was compared with the observed loss in Fig. 11 and shows good agreement up to 400°C above ambient temperatures. The model was not as good in predicting the thermal time constant of device, see Fig. 12. This is not unexpected because the thermal time constant is sensitive to errors in both the thermal conductance and capacitance terms. Thus, a non-linear thermal model, i.e. with temperature-dependent elements, would be better.

[2] For the sake of expedience, we have attributed all of the model error to the capacitance term rather than adjusting the values of all the elements in our lumped system model.

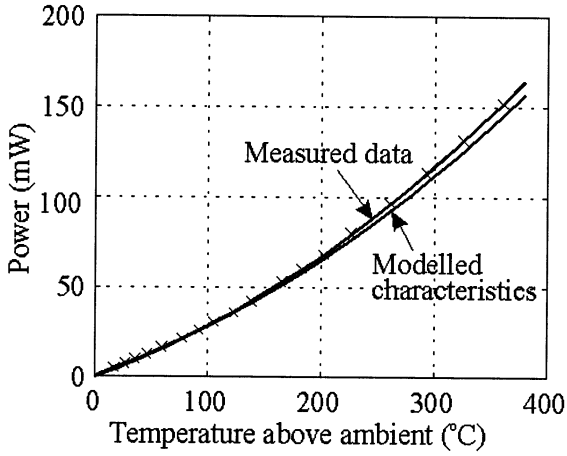

Fig. 11. Comparison of the theoretical power loss (solid lines) of the micro-hotplate from a linear lumped-element model against experimental data.

5. Conclusions

The design of silicon micro-machined hot-plates may be improved through the development of simple thermal models. It has been shown here that a simple lumped-element model can provide a reasonable description of the thermal properties of a micromachined chemoresistive gas sensor with a silicon nitride membrane. It was found that a very low power consumption (40 mW per chemoresistor at 300°C) is achievable in a micro-hotplate and that there is considerable scope to reduce the average value further by using a pulsed mode of operation. The power consumption of the micro-hotplate is well-described by the combination of a first-order conductive loss mechanism and a second-order convective mechanism. Radiation losses are fourth order in temperature and contribute less than 10% to the power loss at operating temperatures below 500°C.

The thermal time constant of the micro-hotplates was measured and found to be very rapid indeed with the hotplate reaching a temperature of 400°C from ambient in less than 4 ms. This fast thermal response suggests that chemoresistive sensors could be temperature-pulsed to decrease their average power consumption but still provide a reading every second. Moreover, rapid temperature cycling also provides the real possibility of employing a single silicon sensor to analyse a multicomponent gas mixture. It has already been shown that the time-frequency analysis of a thermally cycled micro-hotplate coated with a thick tin oxide film can predict the concentrations of both CO and NO_2 in air [9]. Thus, resistive gas sensors employing micro-hotplatess must be an attractive proposition for application in new generations of hand-held gas monitors and small electronic noses.

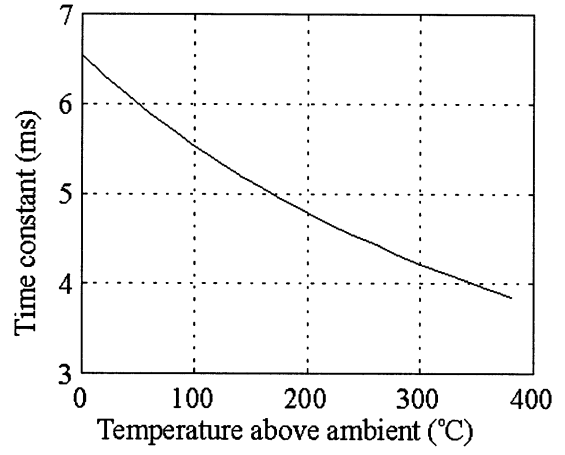

Fig. 12. Comparison of the theoretical thermal time, constant of the micro-hotplate from a linear lumped-element model against experimental data gathered at different temperatures (obtained by driving the micro-heater with a square-wave voltage).

Acknowledgements

The authors thank the Engineering and Physical Research Council and the Health and Safety Executive (Sheffield) for their financial support of a CASE Studentship; the Central Microstructures Facility at the Rutherford Laboratory for mask-plate manufacture; and the Institute of Microtechnology (University of Neuchatel) for processing the wafers.

References

[1] P.T. Moseley, B.C. Tofield, Solid State Gas Sensors, Adam Hilger, Bristol, 1987, pp. 17–31.
[2] Figaro Engineering, Figaro Gas Sensors Products Catalogue, April, 1995.
[3] J.W. Gardner, Microsensors: Principles and Applications, Wiley, Chicester, 1994, p. 331.
[4] V. Demarne, A. Grisel, An integrated low-power thin-film CO gas sensor on silicon, Sensors and Actuators 4 (1991) 539–543.
[5] A.C. Pike, Ph.D. thesis, University of Warwick, Coventry, 1996.
[6] J.W. Gardner, A.C. Pike, N.F. de Rooij, M. Koudelka-Hep, P.A. Clerc, A. Hierlemann, W. Göpel, Integrated array sensor for detecting organic solvents, Sensors and Actuators B 26-27 (1995) 135–139.
[7] P.N. Bartlett, J.M. Elliot, J.W. Gardner, Integrated sensor arrays for dynamic measurement of food flavour release, Meas. Control 30 (9) (1997).
[8] A.J. Chapman, Heat Transfer 4th edn. Macmillan, New York, 1984.
[9] A. Heilig, N. Bârsan, U. Weimar, M. Schweizer-Berberich, J.W. Gardner, W. Gopel, Gas identification by modulating temperatures of SnO_2 based thick film sensors, Sensors and Actuators B 43 (1997) 45–51.

Biographies

Dr. Pike graduated from Warwick University in 1992 with an honours degree in Electronic Engineering. He then carried on at Warwick to study the properties of chemoresistive silicon gas sensors, and was awarded a PhD in 1996. Since then he has been working for Neotronics Scientific Ltd (UK) on the design of electronic nose instrumentation.

Dr. Gardner graduated from Birmingham University in 1979 with a first class honours degree and then studied the properties of thin films at the Cavendish laboratory for his PhD. From 1983 to 1987 he worked first at AEA Technology Ltd and later at Molins Advanced Technology Unit on instrumentation. At Molins he developed a novel opto-electronic sensor that has been packaged in the UK and US for implementation on high speed packaging machinery. Since joining Warwick as a lecturer in 1987, his research interests have been sensor materials, the design of integrated gas array sensors and associated signal processing techniques. In 1989 he received the Esso Centenary Education Award sponsored by the Royal Society and Fellowship of Engineering to pursue his research interests. He was Director of an Advanced Research Workshop on Electronic Noses in 1991 and has published over 200 papers and is an author on 3 technical books in the fields of instrumentation (sensors) and electronic noses. In 1992 he became a Senior Lecturer at Warwick and was an Alexander von Humboldt Fellowship in Germany. Currently, he has a Personal Readership in the Electronics Group, and is the Director of both the Sensors Research Laboratory and the Centre for Nanotechnology and Microengineering at Warwick University. His research interests are silicon sensors and electronic nose instrumentation.